Performance Analysis of the Tube-in-Tube Heat Exchanger in Dilution Refrigerators under Small Flowrates

H.Y. Zu, K. Li, X.T. Wang, Y.N. Wang, J. Shen, W. Dai*

Key Laboratory of Cryogenics, Technical Institute of Physics and Chemistry,
Chinese Academy of Sciences, Beijing, China 100190
University of Chinese Academy of Sciences
Beijing, China 100149

ABSTRACT

Dilution refrigeration is widely used in the frontier research fields of condensed-matter physics, astronomical observation, and quantum computing. Heat exchangers are significant to the normal operation and thermodynamic efficiency of the whole system, especially in the condensation-pump dilution refrigerators with a small driving force. At present, there are few published reports on the comprehensive analysis and quantitative calculation of the continuous tube-in-tube heat exchangers, especially under small flowrates. In this paper, a numerical model is established and the optimum dimensions and thermal performance under small flowrates are calculated using MATLAB. The results show that the Kapitza thermal resistance between the dilute liquid and the wall is the most critical factor, and the axial liquid heat conduction and viscous heating should not be ignored. In the design and optimization of the heat exchanger, the heat transfer area of the dilute fluid should be large enough, and the axial liquid thermal conduction and viscous heating should be restrained to reduce the entropy generation. This study lays a foundation for further design of small condensation-pump dilution refrigerators.

INTRODUCTION

Dilution refrigeration is the most popular subkelvin refrigeration technology supporting many cutting-edge research activities in fields of condensed-matter physics, astronomical observation, and quantum technology. It utilizes ^{3}He atoms that flow from the concentrated phase to the dilute phase, achieving continuous cooling at very low temperatures, ranging from several hundred to a few mK, while providing a relatively large cooling power with no electromagnetic interference. Dilution refrigeration was first proposed by London et al. in 1951 [1] and the first refrigerator was built by Das et al. in 1965 which achieved 220 mK [2]. Through system modifications, primarily to increase the heat transfer area of the heat exchanger, the dilution refrigerator (DR) could achieve 25 mK [3]. After new heat exchangers made from sintered copper and silver powders were put forward, DR temperature was further decreased [4, 5]. At present, the minimum temperature of DRs is 1.75 mK and the cooling power can reach up to 20 μW at 10 mK. The development history of dilution refrigerators is described in detail in reference [6].

Conventional DRs need oil-free mechanical pumps and complex gas-handling systems to achieve room-temperature circulation. There are some disadvantages such as complex system, large footprint,

* Corresponding author, email address: cryodw@mail.ipc.ac.cn

Cryocoolers 22, edited by R.G. Ross, Jr., J.R. Raab and S.D. Miller

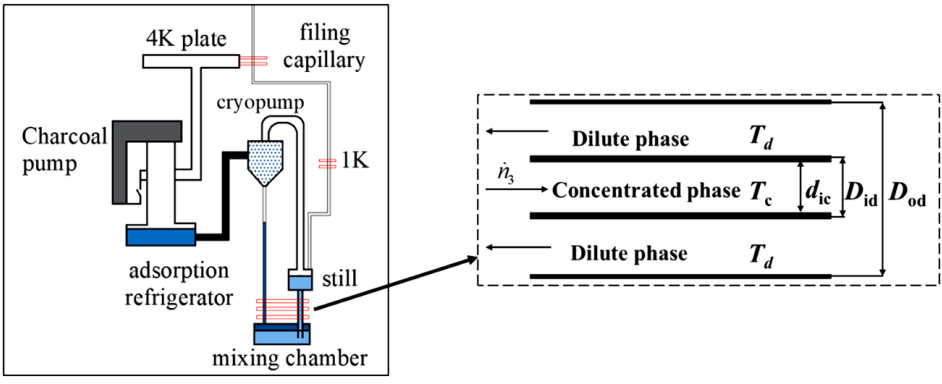

Figure 1. Schematics of the condensation-pump DR [7] and the continuous tube-in-tube heat exchanger.

high pre-cooling heat load, and vibration of oil-free circulating pumps. High cooling power is sometimes not required for many occasions of scientific exploration and high-end instruments with higher requirements of easy operation and compact structure. A condensation-pump dilution refrigerator [7] uses a condensation pump to generate cryogenic ^{3}He circulation without any circulation pumps, as shown in Figure 1. This refrigerator has a compact structure, small volume, and relatively low cost. However, the driving force of the cold cycle is limited by the liquid height difference between the concentrated and dilute fluid and the ^{3}He saturated vapor pressure difference corresponding to the still and cryopump temperature. Under low driving force, the quantitative calculation of the heat exchanger is particularly important. On the one hand, the heat exchanger is one of the key factors to determine the temperature and cooling power. On the other hand, the flow resistance of the heat exchanger is critical to the normal operation of the system. In addition, through analyzing the reported experimental data, the efficiency of the condensation-pump dilution refrigerator [7, 8] can reach 3% of the Carnot efficiency with a temperature difference between 440 mK and 95 mK. Compared with the efficiency of a single-stage ADR, its efficiency is much lower.

The heat exchangers of a DR include continuous tube-in-tube heat exchangers and step heat exchangers with sintered metal powders. While the latter provide better performance at extremely low temperatures, only the continuous tube-in-tube heat exchanger can also produce a lowest temperature below 50 mK. Most previously published research of continuous tube-in-tube heat exchangers is limited to simplified calculation of heat exchange area and how to avoid system instability. Systematic in-depth quantitative calculation is rarely reported.

In this paper, based on quantum fluid properties and heat transfer characteristics at low temperatures, theoretical and numerical models of continuous tube-in-tube heat exchangers are set up. The effect of dimensions such as the length and diameters of the heat exchanger on thermal performance is analyzed. Some parametric studies have also been performed.

THEORETICAL MODEL

The continuous tube-in-tube heat exchanger is a typical counterflow heat exchanger. The concentrated phase flows in the internal tube, and the dilute phase flows in the annular space. In our model, the axial lengths of the concentrated and dilute channels remain equal, as shown in Figure 1.

Momentum Equation

The flow in the heat exchanger is the Poiseuille flow. The pressure drops per unit length of the concentrated liquid and the dilute liquid are

$$-\frac{dp_c}{dl} = \frac{128\eta_c \dot{n}_3 V_{3,c}}{\pi d_{ic}^4} \tag{1}$$

$$-\frac{dp_{\mathrm{d}}}{dl}=\frac{128\eta_{\mathrm{d}}\dot{n}_3V_{3,\mathrm{d}}}{\pi(D_{\mathrm{od}}-D_{\mathrm{id}})^2(D_{\mathrm{od}}^2-D_{\mathrm{id}}^2)} \tag{2}$$

where η_{c} and η_{d} is the viscosity of the concentrated and dilute liquid. $\dot{n}_3$ is the flow rate, mol/s, d_{ic} is the internal diameter of the concentrated channel, D_{id} and D_{od} is the internal and outer diameter of the dilute channel respectively, V_3 is the volume per mol ^{3}He. The molar volume of the concentrated phase equals to the pure ^{3}He, $V_{3,\mathrm{c}}$ =36.84×10^{-6} m^3/mol . The volume per mol ^{3}He of the dilute phase $V_{3,\mathrm{d}}$ is a function of the molar mixture volume V_{m} and the concentration x.

$$V_{3,\mathrm{d}}=V_{\mathrm{m}}/x=V_4^o(1+0.286x)/x \tag{3}$$

V_4^o is the molar volume of pure ^{4}He, 27.58×10^{-6} m^3/mol.

Energy Balance Equation

In steady-state flow, the energy balance of a finite control volume comes from the axial liquid heat conduction Q_{con}, exchanged heat between two fluids q, and viscous heating q_{f}. The energy balance equation is [9]

$$\dot{n}_3\frac{dH}{dl}=-\frac{dQ_{\mathrm{con}}}{dl}+q+q_{\mathrm{f}} \tag{4}$$

The axial liquid heat conduction is

$$Q_{\mathrm{con}}=-kA\frac{dT}{dl} \tag{5}$$

where k is the thermal conductivity of the liquid and A is the crosssectional area.

The thermal resistance between the concentrated and dilute phase in the heat exchanger consists of three parts: Kapitza thermal resistance on the concentrated side, the solid thermal conducting resistance and Kapitza thermal resistance on the dilute side. The temperatures of the solid and liquid are used to calculate the Kapitza thermal resistance due to their large temperature differences. The liquid temperature gradients in the radial direction are neglected because the ratio of the radial liquid thermal resistance to the Kapitza thermal resistance is small, for example <0.003 on the dilute side. The exchanged heat per unit length is

$$q=\mathrm{sign}\times\frac{T_{\mathrm{c}}-T_{\mathrm{d}}}{\frac{4r_{\mathrm{K,c}}}{\pi d_{\mathrm{ic}}(T_{\mathrm{c}}^2+T_{\mathrm{s1}}^2)(T_{\mathrm{c}}+T_{\mathrm{s1}})}+\frac{\ln(D_{\mathrm{id}}/d_{\mathrm{ic}})}{2\pi k_{\mathrm{s}}}+\frac{4r_{\mathrm{K,d}}}{\pi D_{\mathrm{id}}(T_{\mathrm{d}}^2+T_{\mathrm{s2}}^2)(T_{\mathrm{d}}+T_{\mathrm{s2}})}} \tag{6}$$

The concentrated phase rejects heat, sign = -1. The diluted phase absorbs heat, sign = 1. T_{c} and T_{d} are the temperatures of the concentrated and dilute fluid, respectively. T_{s1} and T_{s2} are the wall temperatures on the concentrated side and dilute side. k_{s} is the thermal conductivity of the solid. r_{K} is the Kapitza resistance coefficient, m^{2}K^4/W.

Continuous tube-in-tube heat exchangers are usually made of CuNi alloys. The Kapitza resistance coefficient between the CuNi alloy and the dilute phase $r_{\mathrm{K,d}}$ is [10]

$$r_{\mathrm{K,d}}=0.01(\mathrm{m}^2\cdot\mathrm{K}^4/\mathrm{W}),\ \text{for}\ T<0.2\ \mathrm{K} \tag{7}$$

Lacking the data of the Kapitza resistance coefficient between the CuNi alloy and the concentrated phase, the Kapitza resistance coefficient of the polished Cu-^{3}He [10] is used, which is

$$r_{\mathrm{K,c}}=-0.001\ln(T)+0.0004(\mathrm{m}^2\cdot\mathrm{K}^4/\mathrm{W}),\ \text{for}\ 0.036\mathrm{K}<T<0.45\mathrm{K} \tag{8}$$

Viscous heating per unit length equals to the volume flow rate multiplying the pressure drop per unit length

$$q_{\mathrm{f}}=\dot{n}_3V_3(-dp/dl) \tag{9}$$

After being precooled in the heat exchanger, the concentrated fluid enters the mixing chamber to produce cooling and then flows into the dilute channel. The cooling power of DR equals to the ^{3}He enthalpy difference of the inlet concentrated phase and outlet dilute phase in the mixing chamber

$$Q_{\mathrm{mc}} = \dot{n}_3(H_{3,\mathrm{d}}(x_{\mathrm{s}}, T_{\mathrm{mc}}) - H_3(T_{\mathrm{i}})) \tag{10}$$

where $H_{3,\mathrm{d}}$ and H_3 is the enthalpy per mol ^{3}He in the dilute and concentrated phase. T_{mc} is the temperature of the mixing chamber; x_{s} is the saturated concentration corresponding to T_{mc}, T_{i} is the inlet temperature of the mixing chamber.

Entropy generation

Entropy generation of the heat exchanger mainly comes from non-isothermal heat transfer and viscous loss [11]. Axial non-isothermal heat transfer results from the axial liquid heat conduction. The radial non-isothermal heat transfer comes from the temperature difference between the liquid and solid, which is mainly due to the Kapitza resistance. The entropy generation of radial non-isothermal heat transfer is

$$\dot{S}_{\mathrm{gen},\Delta\mathrm{Tr}} = \frac{Q}{T_{\mathrm{d}}} - \frac{Q}{T_{\mathrm{c}}} = \frac{Q(T_{\mathrm{c}} - T_{\mathrm{d}})}{T_{\mathrm{c}} T_{\mathrm{d}}} \tag{11}$$

where Q is the exchanged heat, W.

The entropy generation of the mixing chamber

$$\dot{S}_{\mathrm{gen,mc}} = -\frac{Q_{\mathrm{mc}}}{T_{\mathrm{mc}}} + \dot{n}_3(S_{\mathrm{F}}(x_{\mathrm{s}}, T_{\mathrm{mc}}) - S_3(T_{\mathrm{i}})) - \frac{Q_{\mathrm{conc,mcin}}}{T_{\mathrm{i}}} - \frac{Q_{\mathrm{cond,mcout}}}{T_{\mathrm{mc}}} \tag{12}$$

S_{F} and S_3 is the entropy per mol ^{3}He of the dilute phase and inlet concentrated phase in the mixing chamber, J/K/mol. $Q_{\mathrm{conc,mcin}}$ and $Q_{\mathrm{cond,mcout}}$ is the inlet and outlet liquid conduction heat of the mixing chamber, respectively.

Taking the heat exchanger and mixing chamber as a whole, the entropy generation (W/K) is

$$\dot{S}_{\mathrm{gen}} = \dot{S}_{\mathrm{gen,mc}} + \dot{S}_{\mathrm{gen,HEX}} = \dot{n}_3(S_{\mathrm{F,out}} - S_{3,\mathrm{in}}) - \frac{Q_{\mathrm{mc}}}{T_{\mathrm{mc}}} - \frac{Q_{\mathrm{conc,in}}}{T_{\mathrm{c,in}}} - \frac{Q_{\mathrm{cond,out}}}{T_{\mathrm{d,out}}} \tag{13}$$

Where S_{in} is the entropy per mol ^{3}He at the inlet of the concentrated channel. $S_{\mathrm{F,out}}$ is the entropy per mol ^{3}He in the dilute phase at the outlet. $T_{\mathrm{c,in}}$ and $T_{\mathrm{d,out}}$ is the inlet temperature of the concentrated channel and outlet temperature of the dilute channel, respectively. $Q_{\mathrm{conc,in}}$ and $Q_{\mathrm{cond,out}}$ is the inlet and outlet axial liquid conduction heat of the heat exchanger.

Liquid property

^{3}He is fermion, and when the temperature is much lower than Fermi temperature T_{F}, the specific heat is proportional to the temperature. In the ^{3}He-^{4}He mixture, ^{3}He can be regarded as the weakly interacting quasiparticle Fermi gas, and ^{4}He can be regarded as the superfluid background supporting ^{3}He atoms. When the temperature is lower than 0.25 K and the ^{3}He concentration is lower than 0.3, the specific heat of the mixture can be regarded as a combination of pure ^{4}He fluid and quasiparticle Fermi gas.

Papers of Kuerten [12] and Chaudry [13] are referred to calculate the thermal properties of fluids. This section only lists several important properties. The enthalpy of the pure ^{3}He fluid [1] (J /mol) is a function of temperature:

[1] Assume the ^{3}He concentration in the concentrated liquid of the heat exchanger is 100%, and the properties of pure ^{3}He fluid are used for calculation.

$$H_3^o = \int_0^T C_3^0(T)dT \tag{14}$$

where C_3^o is the specific heat of pure ^{3}He.

The enthalpy per mol ^{3}He in the dilute phase is the function of temperature and concentration:

$$H_{3,\mathrm{d}} = \mu_3(x,T) + TS_{\mathrm{F}}(x,T) + \frac{1-x}{x}TS_4^o(T) \tag{15}$$

μ_3 is the chemical potential of ^{3}He, J/mol. S_{F} is the entropy of quasiparticle fermi gas. S_4^o is the entropy of pure ^{4}He.

The superfluid ^{4}He is stationary and the chemical potential of ^{4}He is equal everywhere, which is an important basis to determine the temperature and concentration distribution. Because the hydrostatic pressure is much smaller than the osmotic pressure, it is ignored to simplify the calculation. ^{4}He chemical potential μ_4 (J/mol) can be expressed as

$$\mu_4(T,x) = -V_4^o(p_{\mathrm{f}}(T) + \Pi(T,x)) = \mathrm{const} \tag{16}$$

where p_{f} is the fountain pressure. Π is the osmotic pressure.

The data of the ^{3}He thermal conductivity is obtained from HE3PAK [14], and the data of the thermal conductivity of the dilute phase k_{d} is obtained from Pobell's book (5% ^{3}He in ^{4}He) [10].

The viscosity of pure ^{3}He η_3 [15] is

$$\eta_3 = c_1/T^2 + c_2/T^{1.5} + c_3/T + c_4 \tag{17}$$

Eq. (17) applies to the temperature range from 3 mK to 3.3157 K. c_1, c_2, c_3 and c_4 are coefficients and the values are from reference [15].

The viscosity of dilute phase η_{d} is obtained by fitting the data in Ref. [10], and the fitting formula is

$$\eta_{\mathrm{d}}/T^2 = (4.2911T^2 + 0.1909T + 0.0271)\times 10^{-6} \tag{18}$$

The data in the literature are applicable to 15-100 mK, and this paper assumes that the formula is applicable to 15-200 mK.

NUMERICAL MODEL

The numerical model is set up to calculate the thermal performance. The heat exchanger is regarded as a one-dimensional model, and divided into n-1 segments (n points) along the length. The mesh is shown in Figure 2**.** Using MATLAB, the calculation procedure is shown in Figure 3.

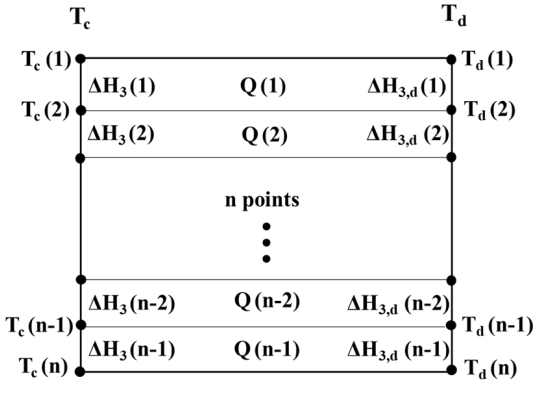

Figure 2. The mesh of the heat exchanger.

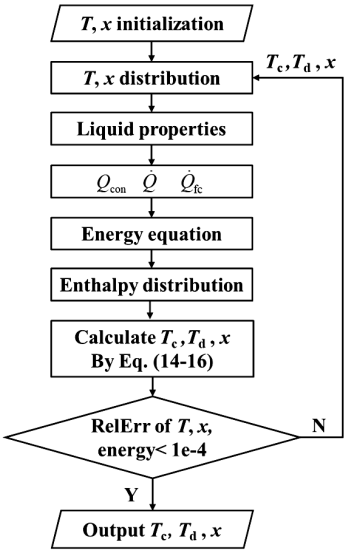

Figure 3. The procedure of the numerical simulation.

The working conditions[2] are as follows: the flow rate of ^{3}He is 7×10^{-6} mol/s, inlet temperature of the concentrated phase is 350 mK, and the cooling temperature T_{mc} is 100 mK. The boundary conditions are as followed:

$$T_c(1) = 350 \text{ mK} \tag{19}$$

$$T_d(n) = T_{mc} = 100 \text{ mK} \tag{20}$$

$$x(n) = x_s(T_{mc}) \tag{21}$$

The grid independence is verified. Taking L=0.583 m, d_{ic}=0.5 mm, D_{id} =0.7 mm, D_{od} =1.2 mm as an example, the relative error of the simulation results between n=71 and n=61 is lower than 0.01%. The mesh number 70 is selected.

SIMULATION RESULTS

Size Optimization

Heat Transfer Area

The heat transfer area between the dilute phase and the wall is the key factor. The performances at different heat transfer areas are investigated by fixing d_{ic}=0.5 mm, D_{id}=0.7 mm, D_{od}=1.0 mm, and increasing L from 0.2 m to 0.6 m. The calculation results are shown in Figure 4. As L increases, the heat transfer area increases. The outlet temperature of the concentrated channel decreases and the cooling power of the mixing chamber increases, while the outlet temperature of the dilute channel rises slightly. When L = 0.5 m, the outlet temperature of the concentrated channel is very close to the mixing chamber. If the length is further increased, the outlet temperature of the concentrated phase almost unchanges, while the entropy generation increases. With the overall consideration of the cooling power and the entropy generation, the heat transfer area of 11 cm^2 on the dilute side when L = 0.5 m is selected as the final heat transfer area.

Diameter Determination

The performances under constant heat transfer area and changing diameter D_{id} are investigated. The fixed diameter relationships are D_{id}-d_{ic}=0.2 mm (equal to the thickness of the internal tube) and D_{od} - D_{id} =0.4 mm. D_{id} increases from 0.6 mm to 0.8 mm and L decreases

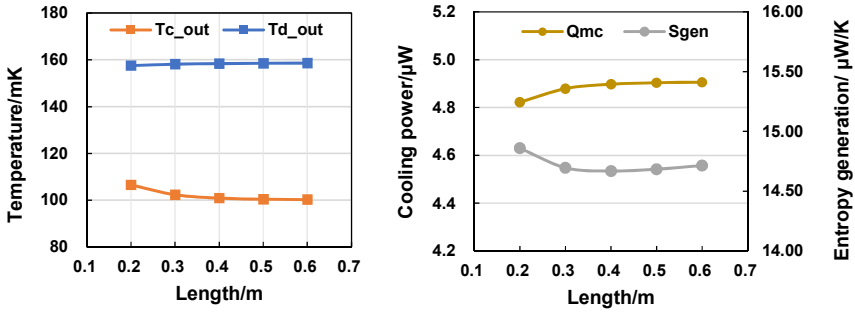

Figure 4. The thermal performances with the changing length of the heat exchanger.

Table 1 The dimensions of the heat exchanger with constant $D_{id} \cdot L$

L/m	d_{ic} /mm	D_{id} /mm	D_{od} /mm
0.583	0.40	0.60	1.00
0.500	0.50	0.70	1.10
0.438	0.60	0.80	1.20

from 0.583 m to 0.438 m. The dimensions are listed in Table 1. The results are shown in Figure 5-6. As D_{id} increases, the outlet temperature of the concentrated phase is almost unchanged, but the outlet temperature of the dilute phase rises slightly due to the increasing of the axial liquid thermal conduction. As D_{id} increases, both the pressure drop and the viscous heating decrease. The entropy generation of the radial non-isothermal heat transfer decreases slightly, but the entropy generation of the axial liquid heat conduction increases and thus the total entropy generation increases. Considering cooling power and entropy generation, D_{id} = 0.6 mm is selected.

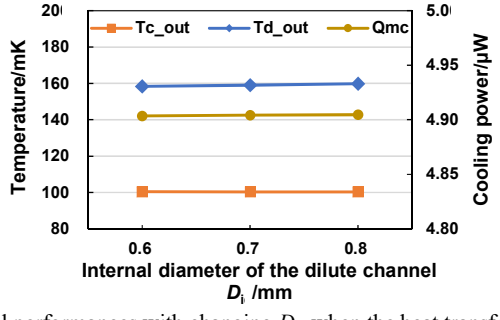

Figure 5. The thermal performances with changing D_{id} when the heat transfer area is constant.

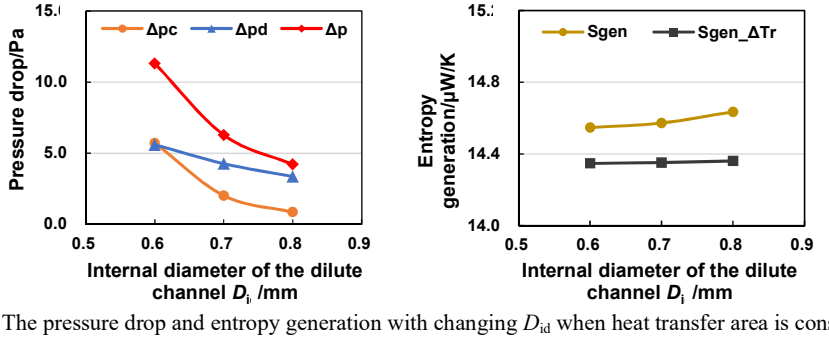

Figure 6. The pressure drop and entropy generation with changing D_{id} when heat transfer area is constant.

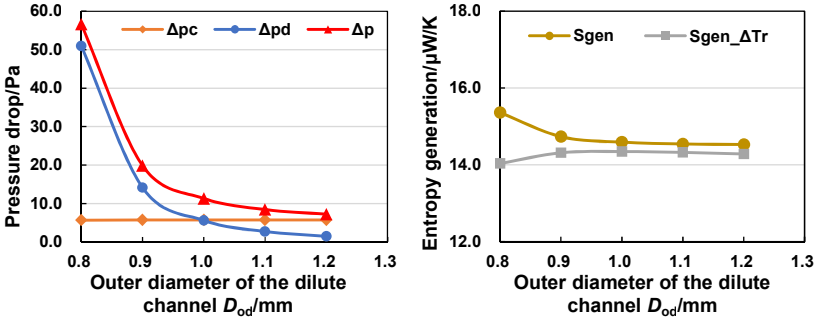

Figure 7. The pressure drop and entropy generation with the outer diameter of the dilute phase.

Based on the above dimensions, the influence of the outer diameter D_{od} of the dilute channel on the pressure drop and entropy generation is investigated. The results are shown in Figure 7. With D_{od} increasing, the pressure drop decreases, and thus the viscous heating decreases. The entropy generation of radial non-isothermal heat transfer increases, while the total entropy generation decreases and approaches a constant value. Considering the pressure drop and entropy generation, the optimal dimensions are determined as d_{ic}=0.4 mm, D_{id} =0.6 mm, D_{od} =1.2 mm, and L =0.583 m.

Performance with the Optimal Dimensions

The performance of the optimal heat exchanger is calculated. Figure 8 shows the distributions of the temperature, concentration and enthalpy flow along the length of the heat exchanger. The specific heat of ^{3}He in the dilute phase is larger than that in the concentrated phase, and thermal equivalent mismatch appears. The enthalpy flow of the dilute phase is much larger than that of the concentrated phase, as shown in the right side of Figure 8. The temperature of the concentrated phase changes greatly, and the temperature gradient along the length direction is larger. The dilute phase in the mixing chamber is saturated, where the concentration is largest. Since the ^{4}He chemical potential in the dilute channel is equal everywhere, the ^{3}He concentration keeps decreasing as the dilute temperature increases from the mixing chamber to the outlet of the dilute channel. The outlet concentration is 5.68%. In addition, the entropy generation is analyzed to show the thermodynamic performances. Figure 9 shows the distribution of the entropy generation per unit length caused by the radial non-isothermal heat transfer in the heat exchanger. The thermal resistance between the dilute phase and wall is the largest because of the larger Kaptiza resistance coefficient and lower temperature, which results in the larger radial temperature difference. Therefore, the corresponding entropy generation is much larger.

Table 2 summarizes the performance of the heat exchanger. The heat exchanger can cool the concentrated fluid from 350 mK to 100.3 mK, and the outlet temperature of the dilute phase is 159.4 mK. The cooling power of the mixing chamber is 4.90 μW at 100 mK. The total fluid

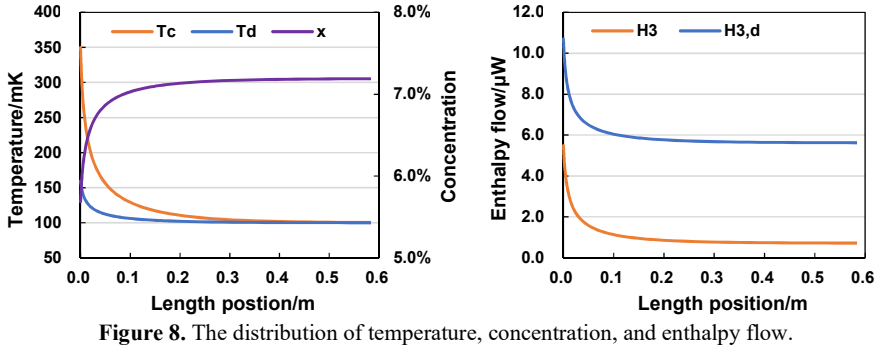

Figure 8. The distribution of temperature, concentration, and enthalpy flow.

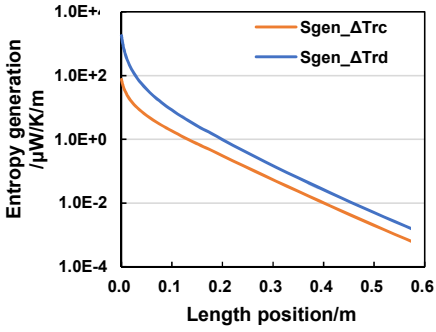

Figure 9. The entropy generation per unit length caused by the radial non-isothermal heat transfer.

Table 2 The performances of the optimized heat exchanger.

Physical properties	Value
Outlet temperature of the concentrated channel	100.3 mK
Outlet temperature of the dilute channel	159.4 mK
Cooling power	4.90 μW
Pressure drop of the concentrated fluid	5.72 Pa
Pressure drop of the dilute fluid	1.47 Pa
Entropy generation of the heat exchanger	14.53μW/K
Entropy generation due to radial non-isothermal heat transfer	14.28 μW/K

pressure drop is 7.20 Pa. The total entropy generation of heat exchanger and mixing chamber is 14.53 μW/K, where the contribution of the mixing chamber is nearly zero. The entropy generation of radial non-isothermal heat transfer is 14.28 μW/K, accounting for 98.3% of the total entropy generation. The high temperature end of the heat exchanger has a large fluid temperature gradient and a large proportion of axial liquid heat conduction. Meanwhile, the viscosity of fluid increases with the decrease of temperature, and the proportion of viscous heating at the low temperature end is larger. Therefore, in the calculation of heat exchanger, the axial liquid heat conduction and viscous heating should be considered to ensure the accuracy of calculation.

CONCLUSION

In this paper, the theoretical and numerical model of the continuous tube-and-tube heat exchanger in the dilution refrigerator are established, and the corresponding simulations under small flowrates are carried out. It is found that:

(1) When the diameter of the heat exchanger increases, the pressure drop and the viscous heating decrease, but the axial thermal conductivity of the liquid increases. The influence of viscous heating and axial liquid heat conduction on the heat transfer and irreversibility can not be ignored under small flowrates.

(2) The dimensions of the heat exchanger are the compromise of the cooling power and entropy generation.

(3) The non-isothermal heat transfer due to the Kapitza thermal resistance on the dilute side is the key factor affecting its performances.

The optimal dimensions of d_{ic}= 0.4 mm, D_{id} = 0.6 mm, D_{od} =1.2 mm, L = 0.583 m are obtained, and the corresponding heat transfer performances are quantitatively analyzed. The optimized heat exchanger can cool the concentrated phase from 350 mK to 100.3 mK, and the cooling power is 4.90 μW at 100 mK. In the design and optimization of heat exchanger, the heat transfer area of the dilute phase should be increased, and the axial liquid heat and viscous heating should be restrained to reduce the entropy generation.

ACKNOWLEDGMENT

We thank A.T.A.M. de Waele for valuable discussions and critical comments.

This work is financially supported by National Key R&D Program of China (No. 2021YFC2203303) and the National Natural Science Foundation of China (No. 52176027).

REFERENCES

1. London, H., *Proceedings of International Conference on Low Temperature Physics (LT2)*, Oxford, UK (1951), pp. 157.
2. Das, T.P., R.D.B. Ouboter, K.W. Taconis, *Proceedings Ninth International Conference on Low-Temperature Physics*, Ohio, US (1965), pp. 1253.
3. Neganov, B., N. Borisov, M. Liburg, "A Method for Obtaining Low Temperatures Based on Dissolution of ^{3}He in ^{4}He," *JETP*, Vol.50 (1966), pp. 1445-57.
4. Vilches, O.E., J.C. Wheatley, "Experiments on dilution of ^{3}He with ^{4}He at very low temperatures," *Physics Letters A*, Vol.24, No.9 (1967), pp. 440-2.
5. Radebauge, R., J.D. Siegwarth, J.C. Holste, "Heat transfer between sub-micron silver powder and dilute He^3-He^4 solutions," *Proceedings of the Fifth International Cryogenic Engineering Conference*, Kyoto, Japan (1974), pp. 242-5.
6. Zu, H., W. Dai, A.T.A.M. de Waele, "Development of dilution refrigerators—A review," *Cryogenics*, Vol.121 (2022), pp. 103390.
7. Prouvé, T., N. Luchier, L. Duband, "Pocket Dilution Cooler," *Cryocoolers 15*, ICC Press, Boulder, CO (2009), pp. 497-503.
8. Teleberg, G., S.T. Chase, L. Piccirillo, "A miniature dilution refrigerator for sub-Kelvin detector arrays," *Proceedings of SPIE*, (2006), pp. 6275OD-1-9.
9. Siegwarth, J., R. Radebaugh, "Analysis of Heat Exchangers for Dilution Refrigerators," *Review of Scientific Instruments*, Vol.42 (1971), pp. 1111-9.
10. Pobell, F., *Matter and Methods at Low Temperatures*, Third ed, Springer, Berlin Heidelberg (2007), pp. 467.
11. Bejan, A., *Advanced Engineering Thermodynamics*, Fourth ed, John Wiley & Sons Inc., Hoboken, New Jersey (2006), pp. 782.
12. Kuerten, J.G.M., C.A.M. Castelijns, A.T.A.M. de Waele, H.M. Gijsman, "Thermodynamic properties of liquid ^{3}He-^{4}He mixtures at zero pressure for temperatures below 250 mK and ^{3}He concentrations below 8%," *Cryogenics*, Vol.25, No.8 (1985), pp. 419-43.
13. Chaudhry, G., J.G. Brisson, "Thermodynamic Properties of Liquid ^{3}He-^{4}He Mixtures Between 0.15 K and 1.8 K," *Journal of Low Temperature Physics*, Vol.155, No.5-6 (2009), pp. 235-89.
14. Huang, Y.H., G.B. Chen, V.D. Arp, "Helium-3 Thermophysical Properties Program – He3Pak, Version 2.0," Shanghai Jiao Tong University (2009), available from Horizon Technologies, Littleton, CO, USA, https://htess.com.
15. Huang, Y., Q. Yu, Q. Chen, R. Wang, "Viscosity of liquid and gaseous helium-3 from 3mK to 500K," *Cryogenics*, Vol.52, No.10 (2012), pp. 538-43.